MNRAS **000**, 1–?? (2019) Preprint 3 August 2019 Compiled using MNRAS LATEX style file v3.0

Dark matter halo shapes at $z = 0$ in the Auriga simulations

Jesus Prada,[1]⋆ Jaime E. Forero-Romero,[1] Robert J. J. Grand,[2] Rüdiger Pakmor,[2] Volker Springel[2]

[1] *Departamento de Física, Universidad de los Andes, Cra. 1 No. 18A-10, Edificio Ip, Bogotá, Colombia*
[2] *Max-Planck-Institut für Astrophysik, Karl-Schwarzschild-Str. 1, D-85741 Garching, Germany*

Accepted XXX. Received YYY; in original form ZZZ

ABSTRACT

We present shape measurements of Milky Way sized dark matter halos at redshift $z = 0$ in a suite of 30 zoom simulations from the Auriga project. We compare the results in full magnetohydrodynamics against dark matter only simulations and find a strong influence of baryons in making dark matter haloes rounder at all radii compared to its dark matter only counterparts. At distances $\lesssim 30$ kpc, rounder dark matter distributions correlate with extended massive stellar discs and low core gas densities. We measure the alignment between the halo and the disc at different radii and find a high degree of alignment at all radii for most of the galaxies. In some cases the alignment significantly changes as a function of radius implying that the halo shape twists; this effect correlates with recently formed bulges and is almost absent in the dark matter only simulations. In a comparison against observational constraints we find that 20% of halos in our sample are consistent with observational results derived from the Pal 5 stream that favor an almost spherical shape. Including baryons is a required element to achieve this level of agreement. In contrast, none of the simulations (dark matter only nor with baryons) match the constrains derived from the Sagittarius stream that favor an oblate dark matter halo.

Key words: galaxies: evolution — galaxies: formation — galaxies: haloes — dark matter

1 INTRODUCTION

Our physical picture of the Universe as a whole has been shaped by accurate observations and modeling of our own Galaxy. For instance, the study of the Milky Way (MW) morphology and its separation into global kinematic coherent components, such as its disc and bulge, has been used to support the existence of a Dark Matter (DM) component surrounding the Galaxy (Olling & Merrifield 2000; Sofue et al. 2009; Catena & Ullio 2010; Bovy & Rix 2013; Iocco et al. 2015). In other words, explaining the matter budget and kinematic state of the MW also put constraints on the wider cosmological context that made possible its evolution.

A detailed study of the full three-dimensional MW gravitational potential could constrain the properties of the DM halo surrounding our Galaxy and even help to pin down the nature of the DM particle. For instance, the study of fossil records of stellar streams resulting from infalling globular clusters or satellite galaxies that got tidally disrupted by the gravitational potential of the MW, could be translated into tight constrains both on the shape of the dark matter halo in the outer regions of our Galaxy (Johnston 1998; Helmi & White 1999; Tremaine 1999) and also bound the properties of dark matter substructures, which also depend on the microphysics of a given DM particle.

In any case, the observational constraints on the gravitational potential shape must be confronted against the expectations from different galaxy formation models in an explicit cosmological context. For instance, in the current paradigm of a Cold Dark Matter (CDM) dominated Universe galaxies are expected to be hosted by triaxial DM halos. To what extent the CDM expectations are born out by observations in our Galaxy?

This question has been challenging to address because it has been difficult to produce realistic galactic discs in simulations within the CDM context (Navarro & Steinmetz 1997). The success of such enterprise has been based on understanding how baryonic effects, such as stellar feedback and black hole feedback, play an important role in forming a galactic disc resembling the MW. Along the way, different numerical experiments have also shown that the baryonic effects also impact the DM halo shape making it rounder

⋆ E-mail: jd.prada1760@uniandes.edu.co

than it otherwise be in a DM-only simulation (Dubinski 1994; Debattista et al. 2008; Kazantzidis et al. 2010; Abadi et al. 2010; Bryan et al. 2013; Chua et al. 2019; Artale et al. 2019). Another important aspect of the disc-halo relationship dynamics, namely, the radial evolution of the alignment between the stellar disc and the DM halo, has also been explored in some simulations (Bailin et al. 2005; Debattista et al. 2013).

Observational constraints of the dark matter halo have also been in tension and rapidly evolving during the last decade. One can find studies favoring prolate (Banerjee & Jog 2011; Bowden et al. 2016), oblate (Law & Majewski 2010; Deg & Widrow 2013; Vera-Ciro & Helmi 2013) and spherical configurations (Bovy et al. 2016). Constraints from modeling of stellar streams discard the prolate configuration (Law & Majewski 2010; Pearson et al. 2015; Bovy et al. 2016) although some other studies still doubt that stellar streams can be used to constrain the halo shape once other assumptions, such as the density profile, are relaxed (Ibata et al. 2013).

In this paper we analyze the internal DM halo shape in thirty MW type galaxies from state-of-the-art simulations from the Auriga project. These simulations have large enough numerical resolution, and explicit cosmological context and an appropriate feedback physics to produce realistic MW discs. Furthermore, the relatively large number of simulated systems allows us to have a handle on the statistical significance of our results. This paper is structured as follows. In Section 2 we present the most relevant details of the simulations, in Section 3 we present the method that we use to measure the DM halo shape. In Section 4 we present our results focusing on the radial shape trends at $z = 0$ and the alignments with the stellar disc. We discuss our results in Section 5 to place them into the context of other numerical work, explore correlations of the shape with baryonic properties in the disc and finally make a direct comparison against observational constraints for the MW's dark matter halo shape. We finalize with our conclusions in Section 6.

2 NUMERICAL SIMULATIONS

The Auriga project offers cosmological zoom in simulations of MW-sized dark matter halos in a ΛCDM cosmology. This simulations come in two versions: dark matter only and baryonic physics including magetohydrodynamics. A detailed description of the simulations and their disc properties can be found in (Grand et al. 2017). Here we summarize its main features.

The objects in the simulations were selected from a set of 30 isolated halos in the Evolution and Assembly of GaLaxies and their Environments (EAGLE) project (Schaye et al. 2015). These halos were randomly selected from a sample of the most isolated halos at $z = 0$ whose virial mass M_{200} was between $10^{12} M_\odot$ and $2 \times 10^{12} M_\odot$. The cosmological parameters in these simulations correspond to $\Omega_m = 0.307$, $\Omega_b = 0.048$, $\Omega_\Lambda = 0.693$ and a dimensionless Hubble parameter $h = 0.6777$ (Planck Collaboration et al. 2014)

The selected halos were re-simulated at higher resultion by applying a zoom-in technique with varying physical realism using the moving-mesh AREPO code that includes gravity, ideal magnetohydrodynamics, phenomenological descriptions for star formation, chemical enrichment from supernovae and its stellar feedback. (Springel 2010; Pakmor & Springel 2013). The simulation also follows the formation and evolution of black holes together with the Active Galactic Nuclei feedback

The 30 zoom-in halos have a dark matter particle mass of $\sim 3 \times 10^5\,\mathrm{M}_\odot$ while the barynic mass resolution is $\sim 5 \times 10^4\,\mathrm{M}_\odot$. The softening lenght for gravitational force computation for stellar particles and high-resolution dark matter particles is fixed to be 500 h^{-1} pc in comoving coordinates up to $z = 1$, and 396 pc in physical coordinates afterwards. The gravitational softening length for gas cells changes with the mean cell radius but is limited to be larger than the stellar softening lenght and 500 h^{-1} pc comoving. **We refer to this setup as the Level4 resolution. Six of these haloes were also simulated at a higher Level3 resolution that represent an increase by a factor of 8 in mass and 2 in spatial resolution. We use the higher resolution haloes to define a minimal radius above which our results can be considered as converged.** From now on we refer to the haloes simulated with baryonic physics as the MHD sample and to the haloes simulated with dark matter only as the DMO sample.

3 HALO SHAPE MEASUREMENT

The DM halo shape is an estimate of either the isopotential or isodensity surfaces. Observational inference models usually estimate the isopotential contours which are probed by tracers (gas, stars), while simulations work with the isodensity contours which can be directly calculated from particle positions. Furthermore, the density contours in thin shells are very sensitive to the presence of small satellites. For this reason we measure the shape by taking volume-enclosed particles, rather than shell-enclosed. This method yields results in good agreement to the isodensity contours for radii ≤ 140 kpc as explored by (Vera-Ciro et al. 2011).

In particular, we measure the shape using the reduced inertia tensor (Allgood et al. 2006),

$$I_{ij} = \sum_k \frac{x_k^{(i)} x_k^{(j)}}{d_k^2}, \tag{1}$$

where the particle positions are measured from the minimum of the gravitational potential in each halo and each is weighted by the k-th particle distance $d_k^2 = x_k^2 + y_k^2 + z_k^2$.

The diagonalization of this tensor yields the eigenvectors and eigenvalues that represent an ellipsoidal dark matter halo. The axis lenghts of this ellipsoid $a \geq b \geq c$ are the square root of the **I** eigenvalues and the direction of the principal axis are the corresponding eigenvectors

We start the calculations taking into account particles within a sphere of radius $R_{\rm initial}$ and then recharacterize the triaxial parameters by taking into account particles within an ellipsoid of semi-axes $r, r/q, r/s$ and re-scaled distance $d^2 = x^2 + (y/q)^2 + (z/s)^2$, where $q = b/a$ and $s = c/a$ are the previously calculated axial ratios. We repeat this process until the average deviation of semi-axes is less than 10^{-6}. After convergence we define a unique radius R as the geometrical mean of the axial lenghts $R = (abc)^{1/3}$. We use this radial coordinate R to parameterize the spatial changes

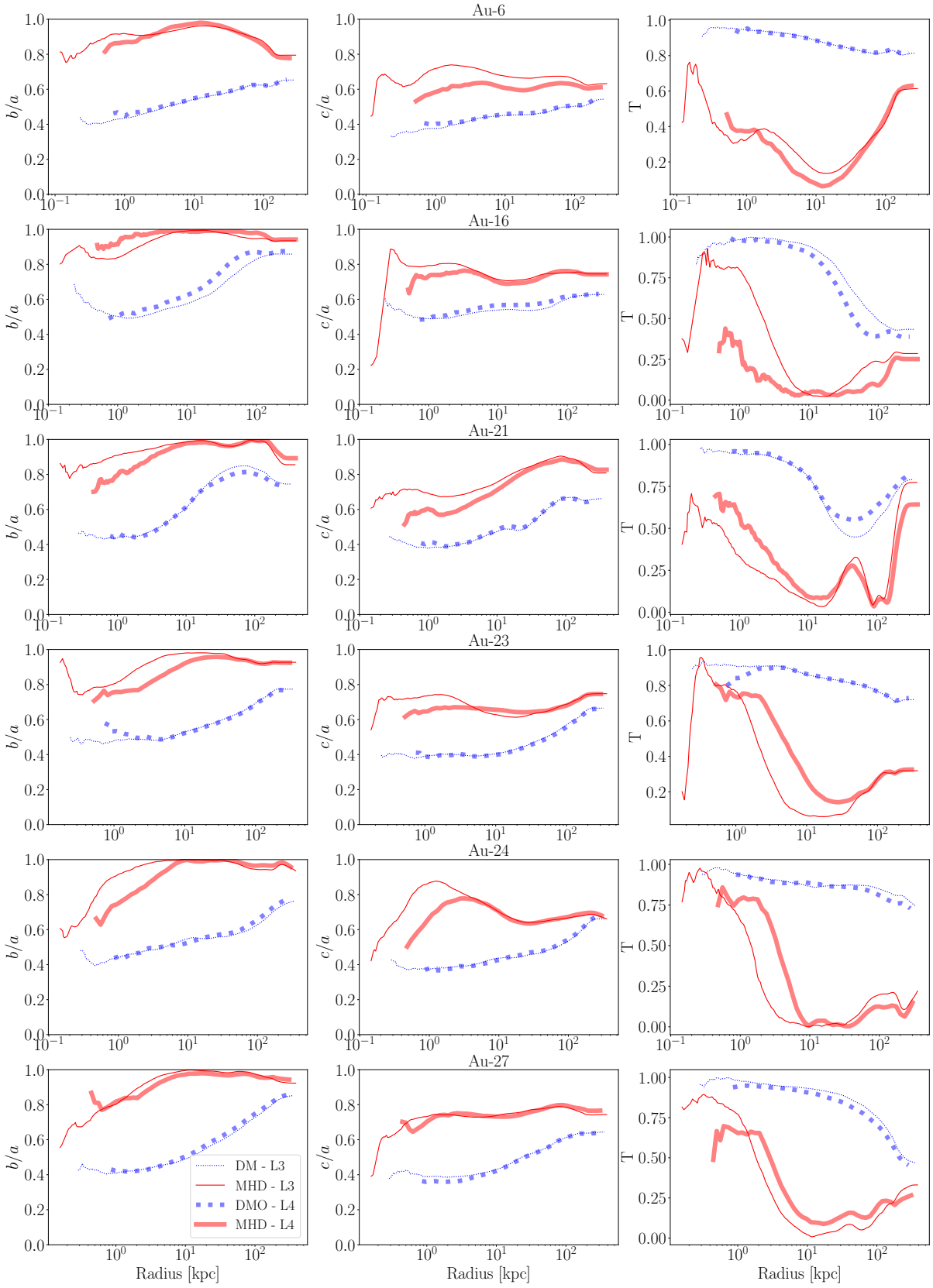

Figure 1. Axial ratios for the six halos simulated at two different resolutions with two different physics (DMO and MHD). In DMO simulations there is a good agreement between the two resolutions (L3 and L4) at all radii down to scales of ≈ 1 kpc from the center. In MHD simulations there are noticeable differences at scales below ≈ 10 kpc. In this paper we only report results at scales larger ≈ 16 kpc ($R_{200}/16$).

Halo	$(b/a)_{16}$	$(c/a)_{16}$	$(b/a)_8$	$(c/a)_8$	$(b/a)_4$	$(c/a)_4$	$(b/a)_2$	$(c/a)_2$	$(b/a)_1$	$(c/a)_1$
Au-1	0.48	0.41	0.52	0.44	0.59	0.48	0.66	0.53	0.72	0.55
Au-2	0.66	0.47	0.72	0.49	0.76	0.51	0.80	0.54	0.79	0.55
Au-3	0.56	0.42	0.61	0.47	0.70	0.55	0.79	0.65	0.85	0.72
Au-4	0.42	0.35	0.47	0.40	0.49	0.43	0.55	0.49	0.59	0.52
Au-5	0.49	0.41	0.53	0.47	0.56	0.51	0.59	0.56	0.66	0.59
Au-6	0.56	0.46	0.58	0.46	0.61	0.49	0.62	0.51	0.65	0.54
Au-7	0.46	0.37	0.45	0.37	0.51	0.40	0.55	0.41	0.62	0.46
Au-8	0.75	0.47	0.84	0.53	0.85	0.58	0.76	0.54	0.82	0.55
Au-9	0.49	0.40	0.52	0.43	0.54	0.45	0.60	0.52	0.65	0.60
Au-10	0.62	0.51	0.61	0.50	0.58	0.49	0.60	0.53	0.65	0.59
Au-11	0.47	0.37	0.36	0.29	0.32	0.28	0.41	0.37	0.47	0.45
Au-12	0.66	0.53	0.76	0.59	0.83	0.66	0.88	0.68	0.94	0.71
Au-13	0.60	0.52	0.61	0.53	0.64	0.54	0.70	0.56	0.73	0.54
Au-14	0.97	0.67	0.95	0.66	0.90	0.64	0.89	0.69	0.87	0.75
Au-15	0.61	0.42	0.65	0.48	0.68	0.52	0.66	0.50	0.70	0.54
Au-16	0.64	0.57	0.73	0.57	0.84	0.58	0.87	0.62	0.88	0.63
Au-17	0.98	0.79	0.98	0.83	0.95	0.84	0.91	0.81	0.93	0.87
Au-18	0.56	0.55	0.57	0.55	0.60	0.57	0.64	0.59	0.62	0.56
Au-19	0.58	0.51	0.59	0.50	0.65	0.54	0.73	0.61	0.80	0.70
Au-20	0.61	0.44	0.68	0.48	0.72	0.51	0.76	0.59	0.81	0.70
Au-21	0.67	0.50	0.75	0.50	0.81	0.61	0.80	0.66	0.74	0.64
Au-22	0.68	0.56	0.71	0.59	0.77	0.63	0.82	0.71	0.83	0.78
Au-23	0.54	0.41	0.58	0.44	0.62	0.49	0.70	0.57	0.77	0.66
Au-24	0.54	0.44	0.57	0.47	0.59	0.49	0.66	0.55	0.75	0.66
Au-25	0.59	0.56	0.66	0.65	0.71	0.66	0.62	0.55	0.69	0.61
Au-26	0.52	0.41	0.58	0.43	0.65	0.43	0.73	0.47	0.75	0.51
Au-27	0.53	0.45	0.61	0.51	0.68	0.56	0.76	0.62	0.84	0.64
Au-28	0.49	0.42	0.49	0.44	0.56	0.48	0.64	0.52	0.74	0.58
Au-29	0.50	0.40	0.56	0.45	0.61	0.48	0.69	0.54	0.72	0.60
Au-30	0.62	0.44	0.77	0.54	0.87	0.58	0.85	0.58	0.75	0.53

Table 1. Axial ratios of Auriga dark matter halos at $z = 0$ at different radii in DMO simulations. The subscripts 16, 8, 4, 2, 1, indicate that the shape was measured at radii of $R_{200}/16$, $R_{200}/8$, $R_{200}/4$, $R_{200}/2$, R_{200}, respectively.

in halo shape we report in the following sections. This is the same method used to estimate the halo shape in the DM-only Aquarius simulations (Vera-Ciro et al. 2011).

Following the convergence criterion by Vera-Ciro et al. (2011) in DM only simulations we restrict the measurement of the ellipsoidal parameters to radii between 1 kpc and R_{200} where R_{200} corresponds to the radius computed enclosing a sphere with 200 times the critical density of the Universe. **However, this scale is similar to the gravitational smoothing length for stellar particles. For this reason we use the Level3 simulations performed at higher resolution to gauge the convergence of the shape measurements in the MHD simulations.**

Figure 1 shows the results for the six halos available both at Level3 and Level4 resolutions. The dotted lines compare the DMO simulations showing that down to scales of 1 kpc the two resolutions yield comparable results (Vera-Ciro et al. 2011). In MHD simulations the situation is different, as expected. The shape ratios b/a and c/a start to differentiate from each other at radii smaller than 15 kpc, tith the exception of Au-27 that shows a good agreement in the shape measuremnts at all radii, Above 15 kpc, the differences between the triaxility values at Level4 and Level3 in MHD simulations are small and never exceed 0.1. For this reason, in order to make the DM halo shape results comparable in DMO and MHD simulations we only report measurements above 15 kpc.

In our results we express the radius as a fraction of R_{200} in order to have a self-consistent dimensionless radius scale across all halos. Given the small variance across halos, each dimensionless radius is associated with a physical value with a mean value and a standard deviation. For instance, over the 30 halos in the sample, the dimensionless radius R_{200} corresponds to a physical distance of 230 ± 16 kpc. Finally, we also measure the alignment of the halo shape against the stellar disc angular momentum. We measure the angular momentum vector using the 10% oldest stellar particles within the virial radius.

4 RESULTS

The main measurements are summarized in Table 1 for the DMO simulations and Table 2 for the MHD simulations. These results are computed at five different radii $R_{200}/16$, $R_{200}/8$, $R_{200}/4$, $R_{200}/2$ and R_{200}. In the following subsections we present and comment in greater detail the results for the triaxility, the halo-disc alignment and the correlations with baryonic disc properties.

4.1 Triaxility

In the DMO sample we find that halos are rounder with increasing radius. The upper panels in Figure 2 illustrate this effect. The contours show a projected DM slice while

Halo	$(b/a)_{16}$	$(c/a)_{16}$	$(b/a)_8$	$(c/a)_8$	$(b/a)_4$	$(c/a)_4$	$(b/a)_2$	$(c/a)_2$	$(b/a)_1$	$(c/a)_1$
Au-1	0.94	0.65	0.96	0.66	0.96	0.70	0.92	0.68	0.91	0.67
Au-2	0.93	0.61	0.95	0.58	0.96	0.61	0.96	0.65	0.88	0.65
Au-3	0.97	0.66	0.96	0.66	0.94	0.70	0.93	0.76	0.94	0.79
Au-4	0.88	0.77	0.82	0.79	0.80	0.76	0.85	0.79	0.83	0.76
Au-5	0.97	0.79	0.94	0.80	0.92	0.81	0.94	0.82	0.94	0.81
Au-6	0.98	0.60	0.96	0.60	0.92	0.63	0.86	0.63	0.78	0.61
Au-7	0.95	0.66	0.95	0.66	0.97	0.68	0.97	0.69	0.96	0.70
Au-8	0.99	0.59	0.97	0.62	0.92	0.66	0.76	0.57	0.83	0.58
Au-9	0.94	0.75	0.93	0.73	0.92	0.73	0.93	0.79	0.92	0.82
Au-10	0.95	0.85	0.94	0.85	0.93	0.85	0.92	0.82	0.91	0.80
Au-11	0.54	0.49	0.55	0.48	0.61	0.53	0.60	0.53	0.62	0.57
Au-12	0.95	0.77	0.88	0.81	0.90	0.84	0.92	0.81	0.95	0.82
Au-13	0.95	0.88	0.96	0.88	0.98	0.82	0.94	0.76	0.82	0.62
Au-14	0.95	0.75	0.93	0.79	0.91	0.80	0.91	0.79	0.93	0.81
Au-15	0.99	0.67	0.98	0.75	0.94	0.79	0.93	0.81	0.88	0.76
Au-16	0.99	0.69	0.99	0.70	0.99	0.74	0.98	0.76	0.99	0.99
Au-17	0.96	0.79	0.96	0.80	0.97	0.82	0.96	0.83	0.96	0.87
Au-18	0.93	0.76	0.92	0.74	0.86	0.72	0.81	0.71	0.74	0.66
Au-19	0.95	0.67	0.91	0.63	0.89	0.63	0.83	0.64	0.85	0.69
Au-20	0.81	0.58	0.91	0.64	0.95	0.71	0.97	0.78	0.86	0.77
Au-21	0.98	0.74	0.97	0.82	0.97	0.87	0.99	0.88	0.99	0.99
Au-22	0.96	0.84	0.93	0.84	0.93	0.85	0.95	0.87	0.97	0.88
Au-23	0.94	0.65	0.96	0.64	0.94	0.65	0.92	0.69	0.93	0.74
Au-24	0.99	0.67	1.00	0.63	0.99	0.65	0.97	0.68	0.98	0.70
Au-25	0.97	0.71	0.96	0.73	0.86	0.74	0.67	0.64	0.71	0.67
Au-26	0.96	0.76	0.97	0.73	0.97	0.70	0.99	0.68	0.97	0.67
Au-27	0.98	0.73	0.97	0.75	0.97	0.79	0.96	0.79	0.95	0.77
Au-28	0.98	0.82	0.94	0.77	0.88	0.73	0.86	0.74	0.93	0.75
Au-29	0.91	0.81	0.89	0.72	0.87	0.69	0.84	0.68	0.85	0.69
Au-30	0.89	0.73	0.78	0.64	0.69	0.53	0.80	0.58	0.91	0.63

Table 2. Same as Table 1 for MHD simulations.

the ellipsoid corresponds to the full 3D shape determination. There we see a highly ellipsoidal halo shape at radii $\sim$ 3kpc that becomes less triaxial at $\approx$ 50 kpc.

We summarize this trend in Figure 3 by plotting the results of all the 30 halos in the DMO sample. The left panel shows every halo in the c/a-b/a plane at two different radii $R_{200}/16$ ($\approx$ 14kpc) and R_{200}. The outer part of the halo is systematically rounder than its inner region. Nevertheless the halo shape can still be considerated to be prolate at all radii.

A different picture presents itself in the MHD sample. There all halos become rounder at all radii than its DMO version. The lower panel in Figure 2 can be directly compared to its MHD counterpart; there we observe how at large radii the halo becomes oblate and almost spherical. The right panel in Figure 3 shows the results for the 30 halos in the MHD sample.

In Figure 4 we summarize the results at different radii using the cumulative distributions for the triaxility parameter T defined as

$$T = \frac{a^2 - b^2}{a^2 - c^2}. \quad (2)$$

The left panel of Figure 4 shows that in the DMO sample the triaxility has a median larger than 2/3 (a typical value that marks the transition from triaxiality to prolateness) at all radii. Furthermore this median value increases as we move towards the inner part of the halo. The right panel shows how the correlations in the MHD simulations go in the opposite direction with respect to DMO result.s There the median triaxility is always smaller than 1/3 (a typical values that marks the transition from triaxility to prolateness) and this median value decreases as we move towards the inner part of the halo.

We now quantify this change in triaxility at the level of individual halos. We compute $\Delta T \equiv T_{\rm MHD} - T_{\rm DMO}$ to quantify the change between the triaxility in the MHD and the DMO simulation. Figure 5 shows the cumulative distribution at the same radii as in Figure 5. From this Figure we observe that at R_{200} all the halos have reduced its triaxility include baryonic physics. At smaller radii this general trend continues, although 2 haloes (Au-11 and Au-17) in our sample increased their triaxility with MHD physics. However, this small fraction correspond to halos that already were outliers in the DMO sample and had triaxilities around 1/3, considerably lower than its parent sample.

4.2 Halo-disc alignments

A common assumption in dynamical models of the MW DM halo is that its angular momentum is perfectly aligned with the stellar disc minor axis. Although it is a reasonable assumption to guarantee the stability of the galactic disc in simplified models of isolated galaxies, this might not perfectly hold in an explicit cosmological context. To examine the degree of validity of this assumption we study in this subsection the alignment between the stellar disc's angular momentum eigenvectors of the dark matter halo shape.

The upper row in Figure 6 shows the alignments be-

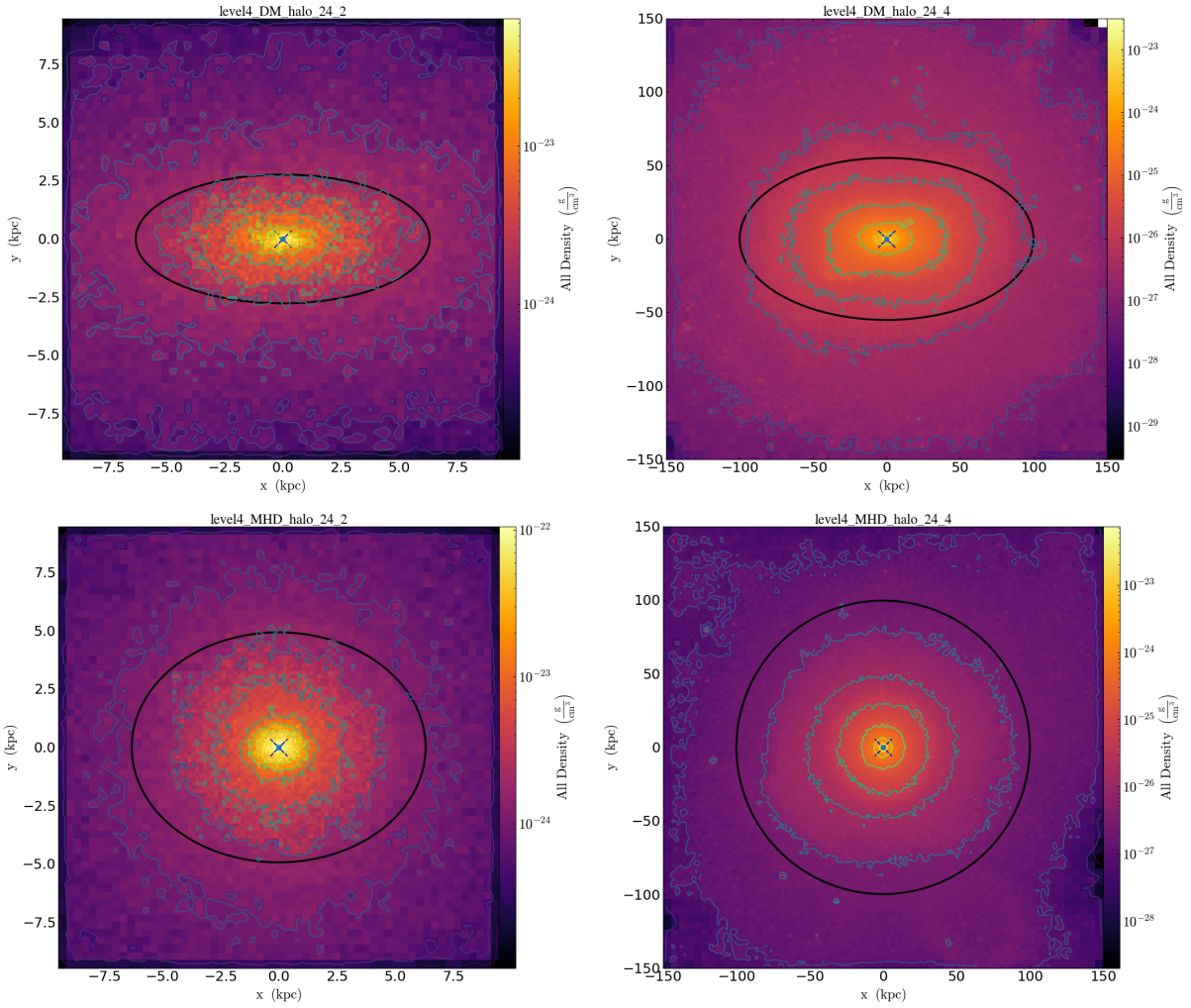

Figure 2. DM density in logarithmic scale within a slice of one tenth of the virial radius. The cut is perpendicular to the short axis of the inertia tensor ellipsoid. The black ellipses show the results of the fitting procedure described in Section 3. Upper/lower panels correspond to DMO/MHD simulations, respectively. Left/right panels show data at small/large radii, respectively. This plot showcases the most noticeable effect in all halos across the Auriga simulations: haloes are rounder at all radii after baryonic physics is included.

tween the major/intermediate/minor axis of the halo and the disc angular momentum as a function of the dimensionless radius at which the halo shape was measured. The upper row shows the angle between the DMO halo and the stellar disk in the MHD simulation. This comparison help us to measure how the shape directions in the dark matter shells change with radius. For the bulk of the sample the lines are horizontal. Only two halos show a significant change of more than 30 degrees across different radii.

The lower row in Figure 6 shows the results for the MHD simulations. The most striking feature of this plot is that most of the discs have their angular momentum aligned with the minor axis of the halo and perpendicular to the intermediate and major axis. The median and the standard deviation of the alignment angles with the major/median/minor axis are 82 ± 14, 82 ± 16 and 19 ± 20 degrees, respectively.

In six halos the alignment changing significantly as a function of radius, this can be seen as a twisting in the shape ellipsoids. As we are dealing with oblate halos $b/a \approx 1$ and the directions corresponding to the medium and major axis could be subject to noise. For this reason, in order to better quantify the twisting for each halo we take the standard deviation of the angle with the minor axis, which should be less susceptible to noise. With this measurement, twisting becomes a global property of the halo, as the standard deviation is measured over the different radii at which we have quantified the alignment.

Figure 7 shows the correlation between twisting at the four different radii at which we have measured the alignments. The median, mean and standard deviation of the twisting are 2, 6 and 8 degrees, respectively. The correlation between twisting and triaxility also changes with radius as measured by the Spearman's rank correlation coefficient. The largest correlation shows with the halo triaxility measured at $0.12R_{200}$. The most important consequence of this changing degree in correlation is that twisting cannot only be explained by large triaxiality values and a possibly noisy determination of the shape axis.

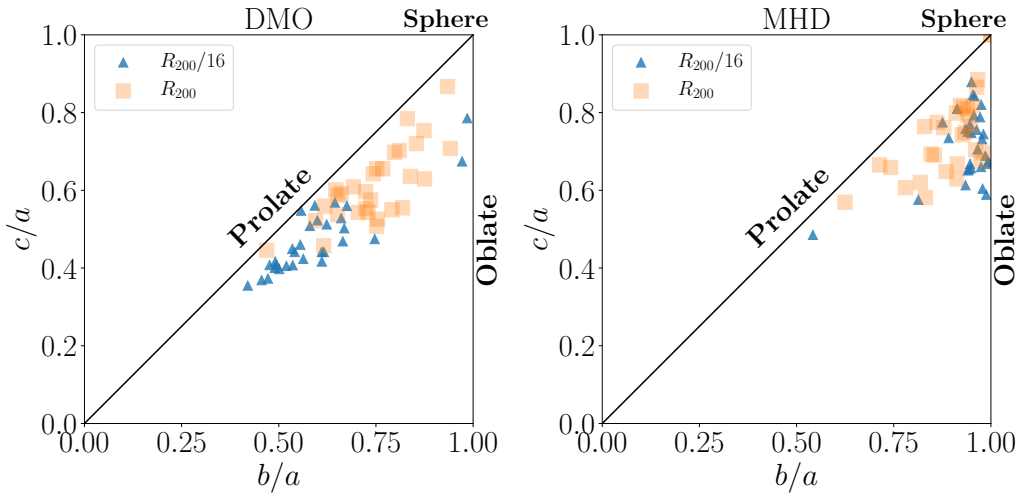

Figure 3. Axial ratios for all simulated halos. Left/right panel corresponds to DMO/MHD simulations, respectively. Triangles (squares) represent the measurements at $R_{200}/16$ (R_{200}) that correspond to physical distances of ≈ 14 kpc (≈ 230 kpc). Here we visualize three main population trends. First, in DMO simulations halos are rounder in the outskirts than in the inner part. Second, halos in MHD are rounder in the inner regions than in the outskirts (opposite to the DMO trend). Third, halos in MHD are rounder than its DMO counterparts. The first and second points are claryfied in Figure 4 through the cumulative triaxility distributions, while the third trend is shown in Figure 5 through the cumulative distribution in the triaxility changes between MHD and DMO at all radii.

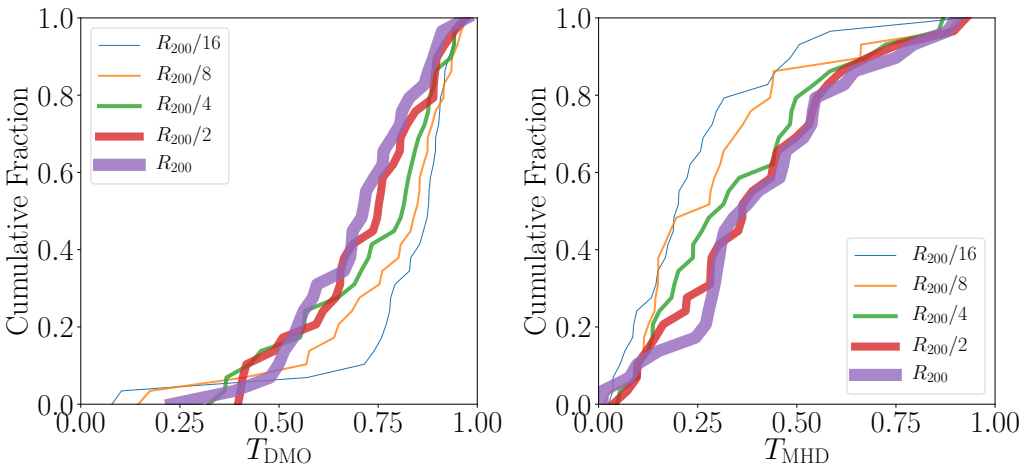

Figure 4. Triaxility cumulative distribution at five different radii. Right/left panel corresponds to DMO/MHD simulations, respectively. In DMO simulations the median triaxiality at all radii is larger than 2/3. Furthermore, the triaxility increases as one moves towards the inner part of the halo. In MHD simulations these trend reverses. The median triaxility at all radii is smaller than 1/3 and the halo is less triaxial as on moves towards the stellar disc.

4.3 Correlation with baryonic disc properties

The presence of baryons produces rounder dark matter halos than its DMO counterpart. To better understand this relationship we quantify the correlation between halo shape with baryonic disc properties. Looking into the measurements already reported by Grand et al. (2017) and Pakmor et al. (2017) we find three baryonic quantities that have the strongest correlation with DM halo triaxiality: the central gas density in a sphere of radius 1kpc, the disc to total mass ratio and the optical radius.

Figure 8 shows the correlations of these quantities with the triaxility at five different radii. We use the Spearmen's rank correlation coefficient to quantify the correlation strength. We find that the strongest correlations are found with the halo shape measured at radii smaller than $0.12R_{200}$. The trend is such that halos with large triaxiality correlate with high gas density and stellar discs with low mass and small size. In turn, massive and large stellar discs within with low density of gas in its core correlate with low halo triaxiliaty.

In some cases, the halo shape also twists in the presence of baryons, as opposed to the situation in DMO simulations where the shape is coherent as a function of radius. In Figure 9 we show the correlation between twisting and the same baryonic properties that showed a high degree of correlation with the triaxility. In this case the disc to total ratio does not have a significant degree of correlation. Instead, the disc

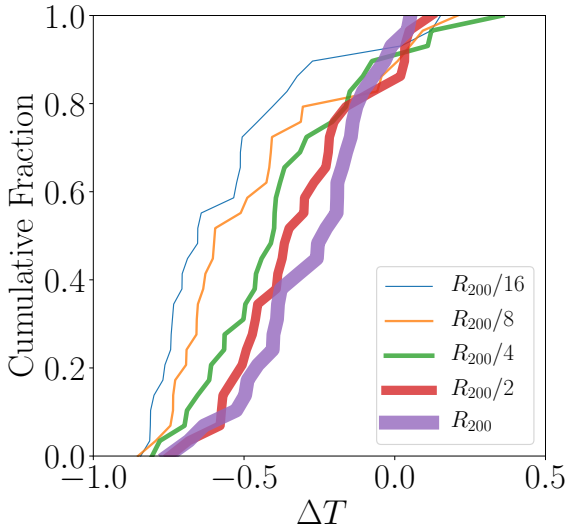

Figure 5. Cumulative distribution for the changes in triaxility in simulations with different physics, $\Delta T = T_{\rm MHD} - T_{\rm DMO}$. At the virial radius all halos become less triaxial in the MHD simulations, the change is stronger towards the halo center. Only two haloes in the sample show the opposite trend of becoming more triaxial (but only at the smaller radii).

optical radius and the gas density at the core are the most correlated. The correlation is such that extended stellar discs with a very low gas density at its core show the most coherent halo shapes.

Recently Borzyszkowski et al. (2017) reported that MW-like DM haloes can be roughly splint into two distinct families: stalled and accreting. Stalled haloes assembled early and have remained almost unchanged in the last 7 Gyr, while accreting halos have been growing constantly. Borzyszkowski et al. (2017) also link this dicotomy to the dark matter filaments feeding the halos. Stalled halos at $z = 0$ are embbeded in a single large thick filament, while accreting halos are pierced by many thinner filaments. To what extent the twisting and high triaxility present in the MHD halos can be linked to this dicotomy? In Figure 10 we show the correlation between the twisting and the age of the bulge, the age of the stellar disc and the DM halo formation redshift. The ages are estimated directly as the mean value in the stellar age distribution for each component, while the formation redshift is defined as the redshif at which the halo already has half of its $z = 0$ mass. In the three cases we find a correlation between ages and twisting that goes in the direction claimed by Borzyszkowski et al. (2017): components with early assembly (i.e. stalled) have a smaller degree of twisting. A detailed study with respect to the cosmic web location is beyond the scope of our paper.

5 DISCUSSION

The first effect that we put in evidence in this paper is the effect of baryons in producing rounder DM halos. This effect has been already widely reported in the literature. It has been found that the strength of the change depends on the numerical resolution, the gas cooling implementation and the models describing star formation and stellar feedback (Bailin et al. 2005; Debattista et al. 2008; Bryan et al. 2013; Butsky et al. 2016; Chua et al. 2019; Artale et al. 2019). The key concept unifying these results is that the baryon distribution influences and correlates with the dark matter halo shape. Indeed, as we presented in the previous section on the correlations with disc properties, we find that the broad tendency is that extended massive stellar discs correlate with spherical dark matter distributions.

We now use the results reported by Law & Majewski (2010) and Bovy et al. (2016) to place our results in an observational context. Law & Majewski (2010) used observations of the Sagittarius tidal stream to constrain the shape of the gravitational potential. Their point of depart is that previous studies that assumed an axisymetric galactic potential were not able to fit all the available dynamic constraints for the Sagittarius stream, therefore making necessary the use of a rigid triaxial potential with coaxial potential ellipsoids for the dark matter component. Their results constrain the triaxility of this potential component. They also translate their results into a triaxiality of the density contours (that could be compared against our results) to be $(c/a) = 0.44$ and $(b/a) = 0.97$ at a radius of $\sim$ 40kpc. They do not report any uncertainties for these two values. Looking at their plots for the quality of fit criterion as a function of dark halo axial scales (their Figure 5), we choose a conservative 10% relative uncertainty. One surprising element in their results is that the major axis of the halo shape is perpendicular to the stellar disc plane.

The results by Bovy et al. (2016) have the same general approach but use instead the GD-1 (Grillmair & Dionatos 2006) and Pal 5 (Odenkirchen et al. 2009) streams to constraint the shape of the dark matter component of the galacic halo potential. They use general models with many degrees of freedom for the galactic potential in order to measure to what extent these two streams are sensitive to the triaxiality of the dark matter halo component. The DM component is written directly as a triaxial density profile with coaxial ellipsoids and the corresponding potential is found by numerical integration. They find that the width of the Pal 5 stream constraints $b/a \approx 1$ and therefore fix it to be $b/a = 1$ exactly. Using that value they report their most stringent constrain of $c/a = 0.93 \pm 0.16$ at a radius of $\approx$ 19kpc from the galactic center.

Figure 11 shows an explicit comparison in the c/a-b/a plane of our results in MHD simulations against the results by Law & Majewski (2010) and Bovy et al. (2016). We find six MHD halos with $b/a < 0.93$ and $c/a > 0.77$ that could be considered consistent with their shape constraints by Bovy et al. (2016), while only one outlier DMO halo is consistent with those constraints. In contrast, none of the simulated halos (MHD nor DMO) is consistent with the results Law & Majewski (2010). The change of triaxility with radius in our simulations cannot account for these two extremely different shape constraints at different radii.

The results by could then place the dark matter halo of our Milky Way as an extreme outlier in the ΛCDM model. This extreme prolateness also correlates with the extreme triaxiality of the 11 classical satellites of the MW ($c/a \approx 0.2$,

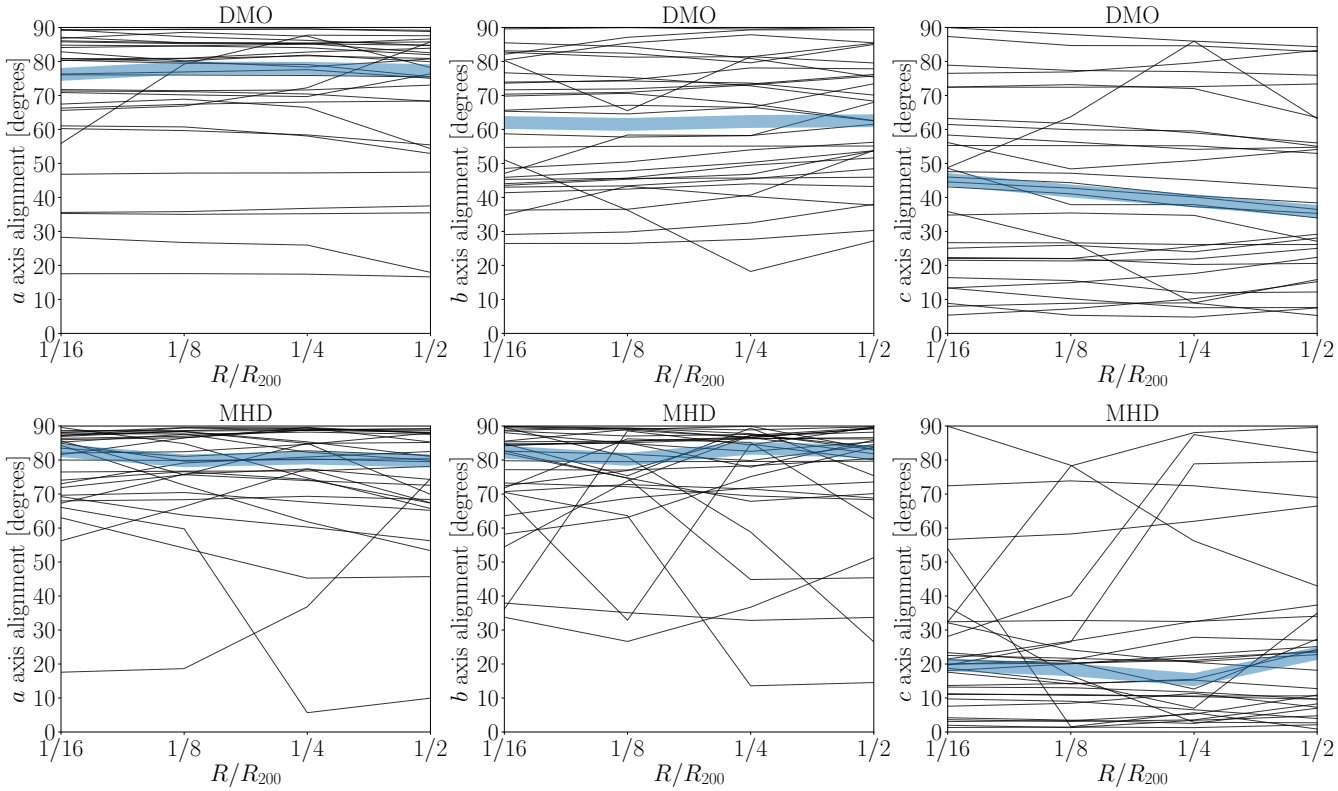

Figure 6. RP: I think the upper row that compares the shape of the halo from the DMO sim with the orientation of the disk in the MHD sim is hard to interpret. Maybe instead show in the first row the angle against a fixed axis (e.g. total angular momentum of the halo?) Angles between the principal axis of the dark matter halo shape and the angular momentum of the stellar disc as a function of the radius at which the halo shape directions are measured. Each panel compares the alignment of the corresponding major/middle/minor axis in the halo. Thin lines correspond to each one of the thirty halos in the sample while the thick line traces the median value at every radius. In the upper row the haloes come from the DMO simulation, showing that the directions in the ellipsoids describing the shape are constant as a function of radius for the most part of the sample. In the lower row the haloes come from the MHD simulation providing a self-consistent comparison with the stellar discs. In this case the dark matter shells twists significantly in 1/5 of the sample. For the remaining haloes the alignment is almost constant as a function of radius.

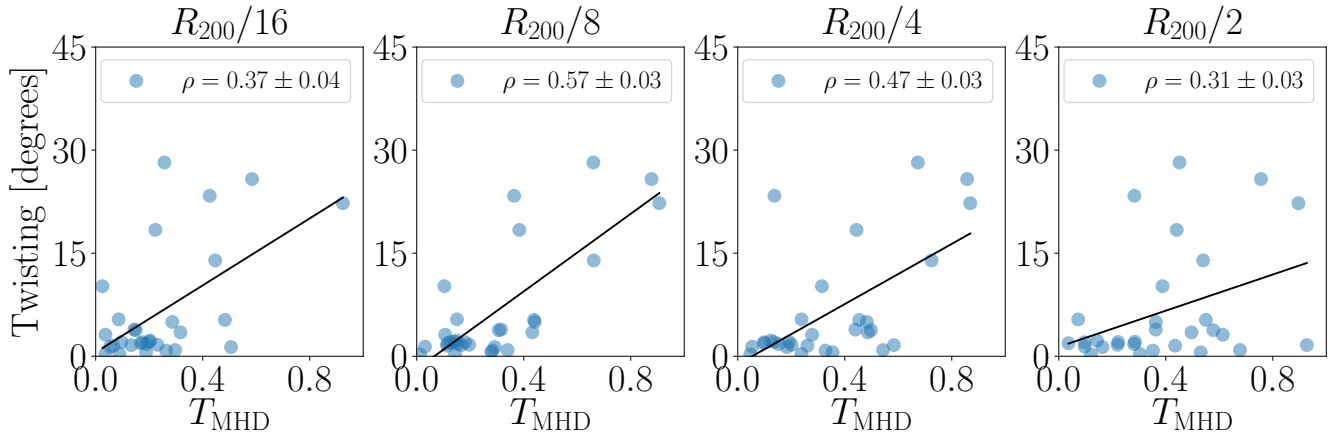

Figure 7. Twisting in the halo-disc alignment (measured as the standard deviation of the alignment angles) as a function of the halo triaxialiy at the radius indicated in each panel's title. The label with the ρ value corresponds to the Spearmans rank correlation coefficient (mean value and uncertainty estimated via jackknife resampling) while the line shows the result of the minimum squares fit to the data. Twisting does not correlate with triaxility in the same way at every radii. The strongest correlation appears around $0.12R_{200}$ (28 ± 2 kpc).

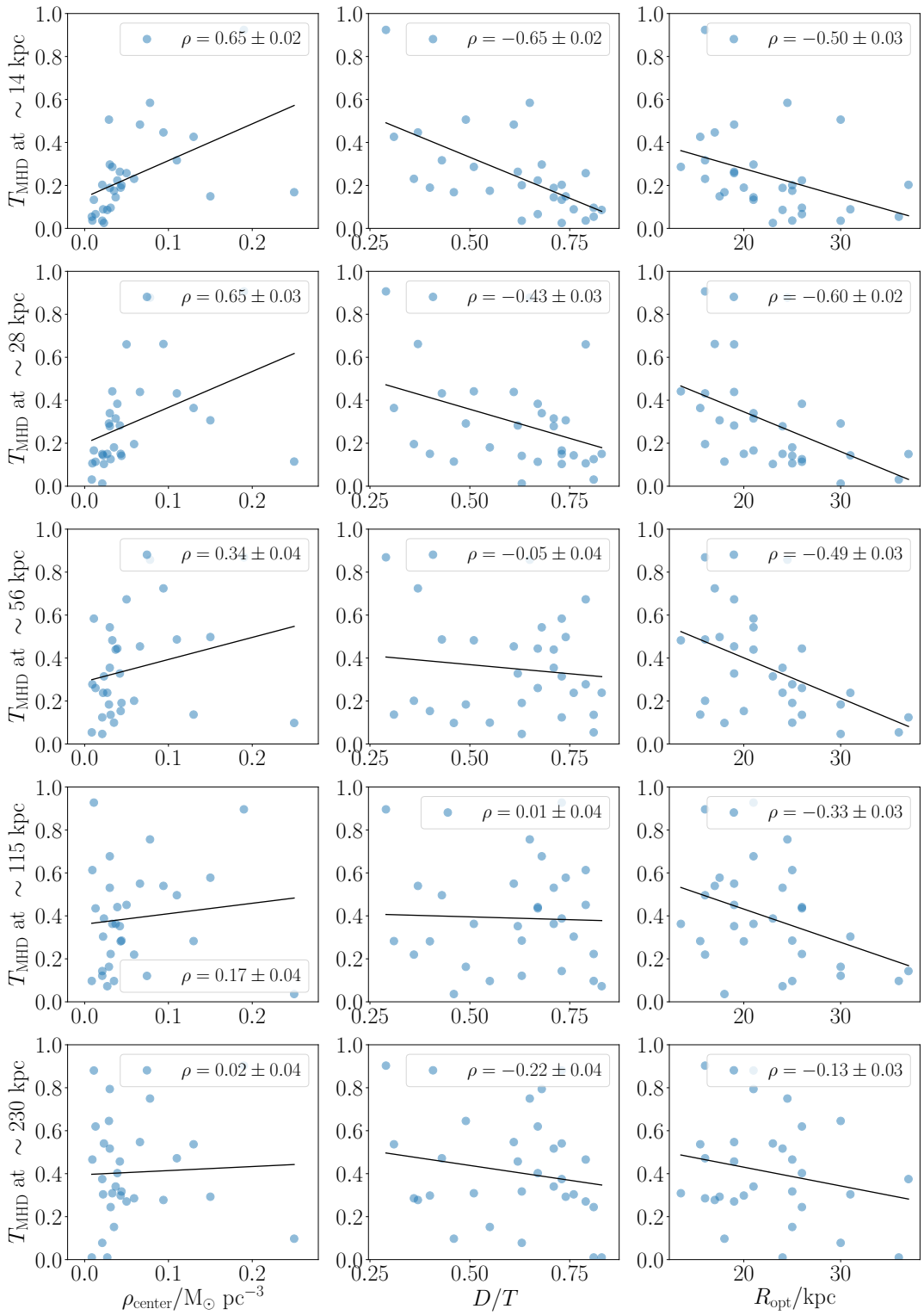

Figure 8. Correlations between the halo triaxility at different radii and baryonic disc properties. The label with the ρ value corresponds to the Spearmans rank correlation coefficient (mean value and uncertainty estimated via jackknife resampling). The line is the best minimum squares fit to a line. The x-axis in the first column is the gas density at the center of the galaxy with in a sphere of radius 1 kpc (Pakmor et al. 2017); the second column shows the disc to total mass ratio and the last column includes the disc optical radius defined to be the radius at which the B-band surface brightness drops below 25 mag arcsec^{-2} (Grand et al. 2017). The largest correlations are found for the two smaller radii ($0.06R_{200}$ and $0.12R_{200}$). Extended and massive stellar discs with a low gas content at its core are correlated with low dark matter triaxilities. The correlation decreases as one approaches larger radii.

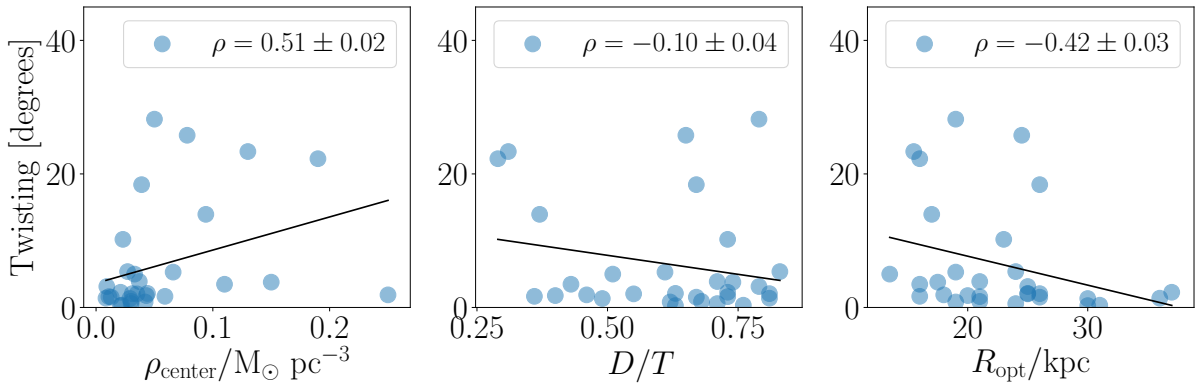

Figure 9. Twisting in the halo-disc alingment as a function of the same baryonic disc properties in Figure 8. The label with the ρ value corresponds to the Spearmans rank correlation coefficient (mean value and uncertainty estimated via jackknife resampling). The line is the best minimum squares fit to a line. In this case the disc to total mass ratio does not correlate with the alignment twisting The gas density at the center and the disc optical radius still show a strong correlation, albeit weaker than what they had with the triaxility.

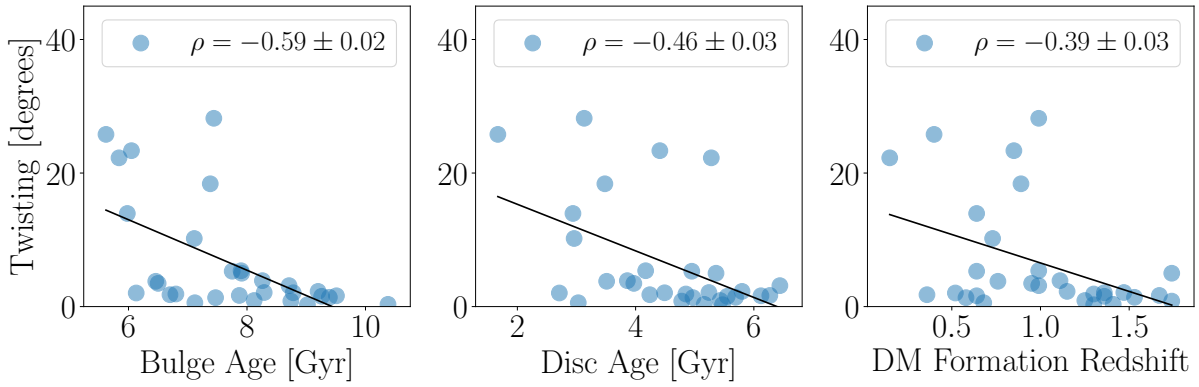

Figure 10. Twisting in the halo-disc alingment as a function of the mean stellar age in the bulge/disc and the lookback formation time of the dark matter halo (time at which it has half of its present mass). The label with the ρ value corresponds to the Spearmans rank correlation coefficient (mean value and uncertainty estimated via jackknife resampling). The line is the best minimum squares fit to a line.

and $b/a \approx 0.9$) measured at larger radii, with an spatial distribution also oriented perpendicular to the MW plane, another highly unusual feature in the ΛCDM (Forero-Romero & Arias 2018).

6 CONCLUSIONS

In this paper we measured the shape of 30 isolated Milky Way sized dark matter haloes simulated in the Auriga project using the zoom-in technique. The halos were with two different setups: dark matter only (DMO) simulation and full magnetohydrodynamics (MHD) including star formation and feedback. We used the shape measurement algorithm by Allgood et al. (2006) on the dark matter halos of these simulations to quantify the halo shape as a function of radius and the degree of aligment between the stellar disc and the halo.

We find that MHD halos are rounder than DMO halos at every radius. MHD halos tend towards more oblate, sometimes almost spherical, shapes ($T < 1/3$), while DMO halos tend towards more prolate shapes ($T > 2/3$). The rounding effect is more noticeable as one moves closer to galactic disc and strongly correlates with baryonic properties of the disc More precisely, the triaxility is smaller for extended and massive stellar discs with low gas densities at its core.

We also measured the alignment of the halo with the stellar disc's angular momentum at different radii. For the majority of the sample the angular momentum is strongly aligned with the minor axis of the halo at all measured radii. However, in some halos the alignment changes noticeably with radius. This alignment evolution implies a radial twisting between the ellipsoids describing the halo shape. We quantify this twist with the standard deviation of the angle between the angular momentum and the halo minor axis at radii below $\leq 0.5R_{200}$ and find that higher gas densities correlate with larger twisting values.

We compared our results against two observational constraints for the dark matter halo shape of the Milky Way. The constraints are at two different radii and come from different observational tracers. We find that 20% halos in the MHD simulations are consistent with the constraints by Bovy et al. (2016) at ≈ 19kpc that correspond to an almost

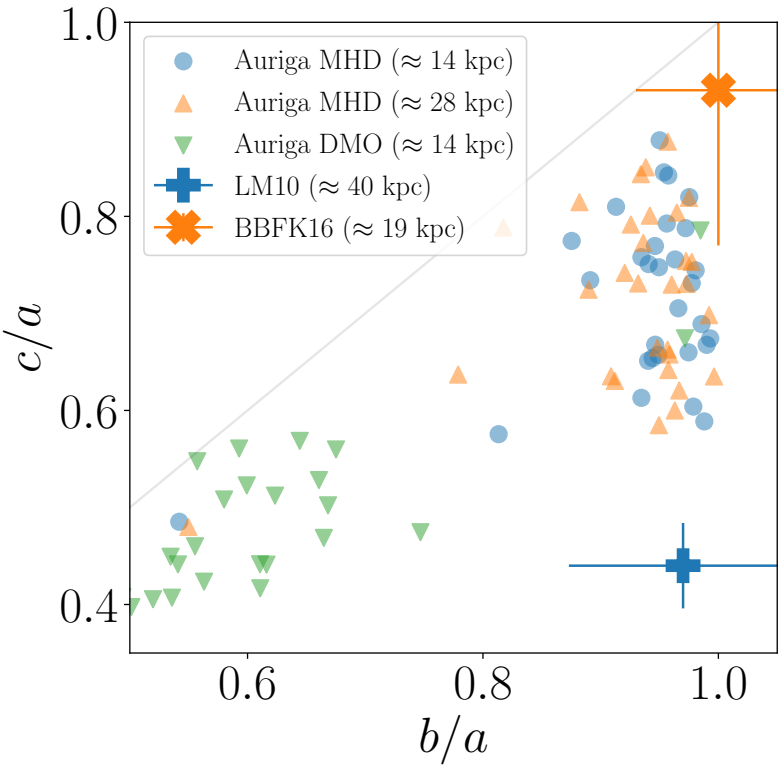

Figure 11. Comparison of our results against observational constraints for the dark matter halo shape in the Milky Way by Law & Majewski (2010) (LM10) and Bovy et al. (2016) (BBFK16). We find that 1/5 of the halos in the MHD sample are consistent with the constraints by Bovy et al. (2016). In contrast, none of the halos in the MHD and DMO seems to be consistent with the results by Law & Majewski (2010).

spherical halo, while none of the halos, either in MHD or DMO, has some overlap with the shape constraints by Law & Majewski (2010) at ≈ 40kpc that is closer to oblate.

Using dark matter only simulations Vera-Ciro et al. (2011) suggested that the current dark matter halo shape strongly correlates with the time evolution of the halo as traced by the shape measured at the virial radius. This effect might no longer hold once baryons are included. The opposed trend of triaxiality in MHD simulation as a function of radius to the DMO simulations together with the twisting effect in some of the halos seems to suggest that that historical buildup memory is not stored in the halo at $z = 0$.

A more complete understanding of the influence of baryons on the different properties we have measured will require at least two more elements. First, an study on how the halo and the disc co-evolved as a function of time. Second, a calibrating the effect of the cosmic web (both dark matter and gaseous) on any evolutionary trend (Forero-Romero et al. 2014; Borzyszkowski et al. 2017; Ganeshaiah Veena et al. 2019) We finalize by suggesting that the twisting density shells we find in some of the halos is feature that deserves to be explored in the process of constraining shape parameters from tidal stream data. The inclusion of a parameterization describing this degree of twisting might relax the conflict between the observational constraints and the numerical results.

ACKNOWLEDGEMENTS

This project has received funding from the European Union's Horizon 2020 Research and Innovation Programme under the Marie Skłodowska-Curie grant agreement No 734374.

REFERENCES

Abadi M. G., Navarro J. F., Fardal M., Babul A., Steinmetz M., 2010, MNRAS, 407, 435
Allgood B., Flores R. A., Primack J. R., Kravtsov A. V., Wechsler R. H., Faltenbacher A., Bullock J. S., 2006, MNRAS, 367, 1781
Artale M. C., Pedrosa S. E., Tissera P. B., Cataldi P., Di Cintio A., 2019, A&A, 622, A197
Bailin J., et al., 2005, ApJ, 627, L17
Banerjee A., Jog C. J., 2011, ApJ, 732, L8
Borzyszkowski M., Porciani C., Romano-Díaz E., Garaldi E., 2017, MNRAS, 469, 594
Bovy J., Rix H.-W., 2013, ApJ, 779, 115
Bovy J., Bahmanyar A., Fritz T. K., Kallivayalil N., 2016, ApJ, 833, 31
Bowden A., Evans N. W., Williams A. A., 2016, MNRAS, 460, 329
Bryan S. E., Kay S. T., Duffy A. R., Schaye J., Dalla Vecchia C., Booth C. M., 2013, MNRAS, 429, 3316
Butsky I., et al., 2016, MNRAS, 462, 663
Catena R., Ullio P., 2010, J. Cosmology Astropart. Phys., 8, 004

Chua K. T. E., Pillepich A., Vogelsberger M., Hernquist L., 2019, MNRAS, 484, 476
Debattista V. P., Moore B., Quinn T., Kazantzidis S., Maas R., Mayer L., Read J., Stadel J., 2008, The Astrophysical Journal, 681, 1076
Debattista V. P., Roškar R., Valluri M., Quinn T., Moore B., Wadsley J., 2013, MNRAS, 434, 2971
Deg N., Widrow L., 2013, MNRAS, 428, 912
Dubinski J., 1994, ApJ, 431, 617
Forero-Romero J. E., Arias V., 2018, MNRAS, 478, 5533
Forero-Romero J. E., Contreras S., Padilla N., 2014, MNRAS, 443, 1090
Ganeshaiah Veena P., Cautun M., Tempel E., van de Weygaert R., Frenk C. S., 2019, MNRAS, 487, 1607
Grand R. J. J., et al., 2017, Monthly Notices of the Royal Astronomical Society, 467, 179
Grillmair C. J., Dionatos O., 2006, ApJ, 641, L37
Helmi A., White S. D. M., 1999, MNRAS, 307, 495
Ibata R., Lewis G. F., Martin N. F., Bellazzini M., Correnti M., 2013, ApJ, 765, L15
Iocco F., Pato M., Bertone G., 2015, Nature Physics, 11, 245
Johnston K. V., 1998, ApJ, 495, 297
Kazantzidis S., Abadi M. G., Navarro J. F., 2010, ApJ, 720, L62
Law D. R., Majewski S. R., 2010, The Astrophysics Journal, 714, 229
Navarro J. F., Steinmetz M., 1997, ApJ, 478, 13
Odenkirchen M., Grebel E. K., Kayser A., Rix H.-W., Dehnen W., 2009, AJ, 137, 3378
Olling R. P., Merrifield M. R., 2000, MNRAS, 311, 361
Pakmor R., Springel V., 2013, MNRAS, 432, 176
Pakmor R., et al., 2017, MNRAS, 469, 3185
Pearson S., Küpper A. H. W., Johnston K. V., Price-Whelan A. M., 2015, ApJ, 799, 28
Planck Collaboration et al., 2014, A&A, 571, A16
Schaye J., et al., 2015, Monthly Notices of the Royal Astronomical Society, 446, 521
Sofue Y., Honma M., Omodaka T., 2009, PASJ, 61, 227
Springel V., 2010, Monthly Notices of the Royal Astronomical Society, 401, 791
Tremaine S., 1999, MNRAS, 307, 877
Vera-Ciro C., Helmi A., 2013, ApJ, 773, L4
Vera-Ciro C. A., Sales L. V., Helmi A., Frenk C. S., Navarro J. F., Springel V., Vogelsberger M., White S. D. M., 2011, MNRAS, 416, 1377